

PAPER

Stub vs. Capacitor for Power Supply Noise Reduction

Toru NAKURA^{†a)}, Student Member, Makoto IKEDA^{††}, and Kunihiro ASADA^{††}, Members

SUMMARY This paper compares a stub and a decoupling capacitor for power supply noise reduction. A quarter-length stub attached to the power supply line of an LSI chip works as a band-eliminate filter, and suppresses the power supply bounce of the designed frequency. The conditions where the stub is more effective than the same-area decoupling capacitor are clarified. The stub will work more efficiently and on-chip integration will be possible on high frequency operation LSIs.

key words: stub, decoupling capacitor, power supply noise, di/dt noise, IR drop

1. Introduction

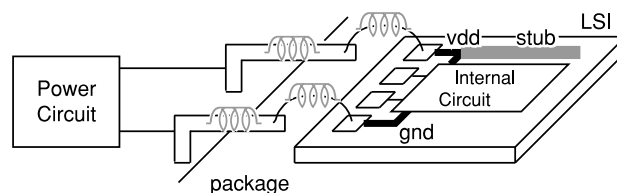
As the process technology advances, the number of the transistors on an LSI chip has been increasing and their high speed operations generate more power supply noise while the low supply voltage reduces the noise margin. Thus, the power supply noise becomes a serious issue for the reliability of the LSI operations.

Recently, a di/dt is becoming one of the dominant source of the power supply bounce along with an IR drop. An EMI noise caused by the di/dt also becomes a serious problem for high speed operating LSIs. In order to suppress the power supply noise caused by the di/dt , some methods, such as a semi-synchronous architecture [1], using a complicated PCB board design [2] have been proposed. These methods, however, make the circuit design complex and difficult. Decoupling capacitors are a conventional method to reduce the power supply bounce, however, they require more die area.

A quarter-length stub attached to the power supply line of an LSI chip works as a band-eliminate filter, and suppresses the power supply bounce of the designed frequency [3], [4] as shown in Fig. 1. Stubs are widely used for impedance matching technique of wireline communications, where the loss of the transmission lines are ignored. Lossy transmission lines have been studied but only for signal wires [5].

This paper compares the stub and the capacitor for the power supply noise reduction.

In Sect. 2, the basic stub theorem and the analytical models are presented. Section 3 shows the simulation results

Fig. 1 Stub di/dt reduction.

of the stub and the capacitor noise reduction effect. Discussions are given in Sect. 4, and Sect. 5 concludes this paper.

2. Analytical Model of Stub and Capacitor

The notations in Table 1 will be used in this paper.

2.1 Stub Basics

As the operation frequency becomes higher and the wavelength of voltage and current get comparable with the wire length, the wire should be considered as a transmission line instead of lumped RC elements. The characteristic impedance Z_0 , the propagation constant γ of the transmission line are

$$Z_0 = \sqrt{\frac{R + j\omega L}{G + j\omega C}} \quad (1)$$

$$\begin{aligned} \gamma &= \sqrt{(R + j\omega L)(G + j\omega C)} \\ &\equiv j\beta_c = \alpha + j\beta_r \end{aligned} \quad (2) \quad (3)$$

where R, L, G, C are the resistance, inductance, admittance representing the dielectric loss, capacitance of the wire, per unit length respectively. $G = 0$ is assumed in this paper.

The input impedance of the transmission line with the length l and the open termination becomes

$$Z_{stub} = Z_0 \frac{\cos \beta_c l}{j \sin \beta_c l} \quad (4)$$

If the transmission line has no loss ($R = 0$) and its length is quarter of the signal wavelength ($\beta_c l = \pi/2$), the input impedance of the stub becomes zero, which is equivalent with an infinite capacitance. When this stub is attached to the power supply line, the voltage fluctuation is suppressed.

The dominant frequency of the switching currents is the clock frequency f_0 . Thus, the stub length adjusted for the clock frequency becomes

Manuscript received May 31, 2004.

Manuscript revised August 21, 2004.

[†]The author is with the Department of Electronic Engineering, The University of Tokyo, Tokyo, 113-8656 Japan.

^{††}The authors are with the VLSI Design and Education Center (VDEC), The University of Tokyo, Tokyo, 113-8656 Japan.

a) E-mail: nakura@silicon.t.u-tokyo.ac.jp

Table 1 Notations.

l	stub length
w	stub width
t	stub, capacitor thickness
d	distance between the upper and the lower plates
A	stub, capacitor area
ρ	resistivity of the wire
δ	skin depth
c	velocity of light in the vacuum
ϵ_0	dielectric constant in the vacuum
ϵ_r	relative dielectric constant
R	resistance per unit length of the stub
L	inductance per unit length of the stub
G	admittance per unit length of the stub
C	capacitance per unit length of the stub
C_{total}	total capacitance of the plates
Z_0	characteristic impedance
Z_{0lf}	characteristic impedance at lower frequency
Z_{0hf}	characteristic impedance at higher frequency
Z_{stub}	stub input impedance
Z_{slf}	stub input impedance at lower frequency
Z_{shf}	stub input impedance at higher frequency
Z_{cap}	capacitor input impedance
f_R	frequency at which skin effects occur
f_C	frequency at which $w = d$
f_D	frequency at which $\omega L = R$
f_S	frequency at which $Z_{slf} = Z_{shf}$
f_B	boundary frequency
γ	propagation constant
α	attenuation constant
β_r	phase constant without loss
β_c	phase constant with loss
η	round trip attenuation factor
τ	time constant from Z_0 to Z_{stub}
Γ_s	reflection coefficient at the stub near end

$$l = \frac{\pi/2}{\beta_{r0}} = \frac{\lambda_0}{4} = \frac{c/\sqrt{\epsilon_r}}{4f_0} \quad (5)$$

where λ_0 , c and ϵ_r are the signal wavelength in the transmission line, the speed of light in vacuum and the relative dielectric constant.

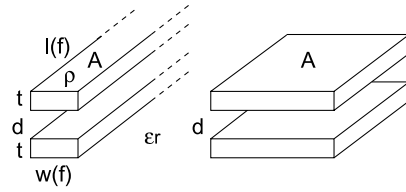
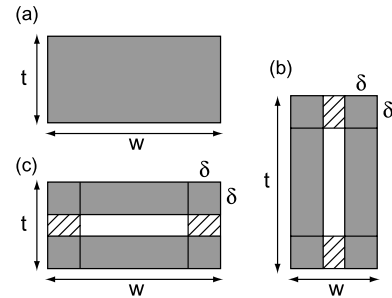
2.2 Stub and Capacitor Impedance

The stub input impedance does not become zero because of the parasitic resistance of the wire. A wider stub reduces the resistance, however, larger area is required and the same-area decoupling capacitor may have the same noise reduction effects. This subsection compares the stub and the capacitor input impedance with the same area A . The thickness of the stub wire is t , the distance between the signal and the gnd line is d , the length and the width are l and w , the resistivity of the stub are ρ and the relative dielectric constant is ϵ_r , as shown in Fig. 2. The relative permeability μ_r is assumed to be 1.

From $A = lw$ and eqn(5),

$$w = \frac{4Af\sqrt{\epsilon_r}}{c} \quad (6)$$

The resistance per unit length R becomes

**Fig. 2** Stub and the same-area decoupling capacitor.**Fig. 3** Current distribution of the wire with the skin effect. (a) $t \leq 2\delta$ or $w \leq 2\delta$, (b) $2\delta < w < t$, (c) $2\delta < t < w$.

$$R = \begin{cases} \frac{\rho}{wt} \times 2 = \frac{\rho c}{2Aft\sqrt{\epsilon_r}} & (t \leq 2\delta \text{ or } w \leq 2\delta) \\ \frac{\rho}{2\delta t} \times 2 = \sqrt{\frac{\rho\pi f}{\epsilon_0 c^2 t^2}} & (2\delta < w < t) \\ \frac{\rho}{w2\delta} \times 2 = \sqrt{\frac{\rho\pi}{16A^2\epsilon_r\epsilon_0 f}} & (2\delta < t < w) \end{cases} \quad (7)$$

where $\delta = \sqrt{2\rho/(\omega\mu_0)}$ is the skin depth, and approximated that the uniform current flows within the skin depth as shown in Fig. 3 gray part, and no current flows at the center and also the hatched part for simplicity. The “ $\times 2$ ” is because the signal and the gnd resistors are merged, and eqn(6), $c = 1/\sqrt{\mu_0\epsilon_0}$ are used. The conditions to become (a), (b) and (c) in Fig. 3 will be described later.

The capacitance per unit length C becomes

$$C = \begin{cases} \frac{\pi\epsilon_r\epsilon_0}{\log \frac{d}{w/2}} = \frac{\pi\epsilon_r\epsilon_0}{\log \frac{cd}{2Af\sqrt{\epsilon_r}}} & (w < d \Rightarrow f < f_C) \\ \frac{w}{\epsilon_r\epsilon_0 d} = \frac{4\sqrt{\epsilon_r}\epsilon_r\epsilon_0 Af}{cd} & (d \leq w \Rightarrow f_C \leq f) \end{cases} \quad (8)$$

$$f_C = \frac{cd}{4A\sqrt{\epsilon_r}} \quad (9)$$

using the parallel cylinder line capacitance model [6] for $w < d$ case and the parallel plate model for $d \leq w$ case. f_C is the frequency at which $w = d$, and eqn(6) is used. Note that discontinuity happens at the transition from the parallel cylinder model to the parallel plate model. Since $c/\sqrt{\epsilon_r} = 1/\sqrt{LC}$,

$$L = \begin{cases} \frac{\log \frac{cd}{2Af\sqrt{\epsilon_r}}}{c^2\pi\epsilon_0} & (w < d \Rightarrow f < f_C) \\ \frac{d}{4\epsilon_0 c A f \sqrt{\epsilon_r}} & (d \leq w \Rightarrow f_C \leq f) \end{cases} \quad (10)$$

The characteristic impedance becomes

$$Z_0 \approx \begin{cases} Z_{0lf} = \sqrt{\frac{R}{j\omega C}} & (\omega L < R \Rightarrow f < f_D) \\ Z_{0hf} = \sqrt{\frac{L}{C}} & (R \leq \omega L \Rightarrow f_D \leq f) \end{cases} \quad (11)$$

$$f_D = \frac{R}{2\pi L} \quad (12)$$

where f_D is the frequency at which $\omega L = R$.

The stub input impedance becomes its characteristic impedance if the total wire resistance $R \times l$ is bigger, while the input impedance goes close to zero if the total wire impedance is small enough, and approximated to $Rl/2$ [7]. Since the total wire resistance reduces as the frequency increases,

$$Z_{stub} \approx \begin{cases} Z_{slf} = Z_{0lf} = \sqrt{\frac{R}{j\omega C}} & (f < f_S) \\ Z_{shf} = \frac{R}{2}l & (f_S \leq f) \end{cases} \quad (13)$$

$$f_S = \frac{\pi c^2 RC}{32\epsilon_r} \quad (14)$$

where f_S is the frequency at which $|Z_{0lf}| = Rl/2$, and (7), (5) are used.

The input impedance of the same-area decoupling capacitor is

$$Z_{cap} = \frac{1}{j\omega C_{total}} = \frac{d}{j2\pi f \epsilon_r \epsilon_0 A} \quad (15)$$

where the resistance is ignored and the ideal parallel plate model is adopted here. The ratio of Z_{stub} and $|Z_{cap}|$ is

$$\left| \frac{Z_{stub}}{Z_{cap}} \right| = \begin{cases} \frac{Z_{slf}}{Z_{cap}} & (f < f_S) \\ \frac{Z_{shf}}{Z_{cap}} & (f_S \leq f) \end{cases} \quad (16)$$

Note that $Z_{slf} < Z_{shf}$ holds for $f < f_S$, so the relation of

$$\frac{Z_{stub}}{Z_{cap}} \leq \frac{Z_{shf}}{Z_{cap}} \quad (17)$$

holds for all frequency. Therefore we use Z_{shf} as the stub impedance for the comparison with the capacitor, and it is a stub-pessimistic evaluation. The ratio becomes

$$\left| \frac{Z_{shf}}{Z_{cap}} \right| = \begin{cases} \frac{\pi c^2 \epsilon_0 \rho}{8tdf} & (t < 2\delta \text{ or } w < 2\delta) \\ \sqrt{\frac{\pi^3 \epsilon_r \epsilon_0 \rho A^2 f}{16t^2 d^2}} & (2\delta < w < t) \\ \sqrt{\frac{\pi^3 c^2 \epsilon_0 \rho}{256d^2 f}} & (2\delta < t < w) \end{cases} \quad (18)$$

using eqn(7), (13) and (15). Note that the ratio decreases as the frequency goes higher on the first and the third conditions while the ratio increases on the second condition as shown in Fig. 4(ii).

The boundary frequency f_B at which $Z_{shf} = |Z_{cap}|$ is

$$f_B = \begin{cases} \frac{\pi c^2 \epsilon_0 \rho}{8td} & (t < 2\delta \text{ or } w < 2\delta) \\ \frac{16t^2 d^2}{\pi^3 \epsilon_r \epsilon_0 \rho t^2 A^2} & (2\delta < w < t) \\ \frac{\pi^3 c^2 \epsilon_0 \rho}{256d^2} & (2\delta < t < w) \end{cases} \quad (19)$$

Here, the relations for t , w and δ are

$$(a) \quad t \leq 2\delta \text{ or } w \leq 2\delta \\ \Rightarrow \begin{cases} \frac{t^3}{A} \leq \frac{16\rho \sqrt{\epsilon_r} \epsilon_0 c}{\pi} \text{ and } f \leq f_{R1} \\ \frac{t^3}{A} > \frac{16\rho \sqrt{\epsilon_r} \epsilon_0 c}{\pi} \text{ and } f \leq f_{R2} \end{cases} \quad (20)$$

$$(b) \quad 2\delta < w < t \\ \Rightarrow \begin{cases} \frac{t^3}{A} > \frac{16\rho \sqrt{\epsilon_r} \epsilon_0 c}{\pi} \text{ and } f_{R2} < f < f_{R0} \end{cases} \quad (21)$$

$$(c) \quad 2\delta < t < w \\ \Rightarrow \begin{cases} \frac{t^3}{A} \leq \frac{16\rho \sqrt{\epsilon_r} \epsilon_0 c}{\pi} \text{ and } f_{R1} < f \\ \frac{t^3}{A} > \frac{16\rho \sqrt{\epsilon_r} \epsilon_0 c}{\pi} \text{ and } f_{R0} \leq f \end{cases} \quad (22)$$

$$f_{R0} = \frac{ct}{4A \sqrt{\epsilon_r}}, \quad f_{R1} = \frac{4\rho c^2 \epsilon_0}{\pi t^2}, \quad f_{R2} = \sqrt[3]{\frac{\rho c^4 \epsilon_0}{4\pi A^2 \epsilon_r}} \quad (23)$$

where f_{R0} , f_{R1} and f_{R2} is the frequency at which $w = t$, $2\delta = t$ and $2\delta = w$, respectively. Note that $w < t$ at $f < f_{R0}$, and $t < w$ at $f_{R0} < f$. Also note that the case (b) $2\delta < w < t$ does not occur when $\frac{t^3}{A} \leq \frac{16\rho \sqrt{\epsilon_r} \epsilon_0 c}{\pi}$, as shown in Fig. 4(i).

The relations which f_B falls within the conditions of eqn(20), where the case (i)-(β), (ii)-(β) or (ii)-(γ) in Fig. 4, are

$$\begin{cases} \frac{t^3}{A} \leq \frac{16\rho \sqrt{\epsilon_r} \epsilon_0 c}{\pi} \text{ and } t \leq \frac{32d}{\pi^2} \\ \frac{t^3}{A} > \frac{16\rho \sqrt{\epsilon_r} \epsilon_0 c}{\pi} \text{ and } t^3 \geq \frac{\pi^4 c^2 \epsilon_r \epsilon_0^2 \rho^2 A^2}{128d^3} \end{cases} \quad (24)$$

and the relations which f_B falls within the conditions of eqn(21), where the case (ii)-(β) in Fig. 4, are

$$\frac{t^3}{A} > \frac{16\rho \sqrt{\epsilon_r} \epsilon_0 c}{\pi} \text{ and}$$

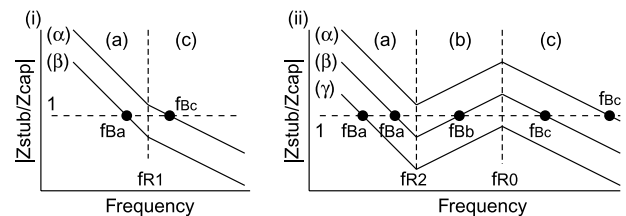


Fig. 4 Simplified graph of $|Z_{stub}/Z_{cap}|$. (i) when $\frac{t^3}{A} \leq \frac{16\rho \sqrt{\epsilon_r} \epsilon_0 c}{\pi}$, and (ii) when $\frac{t^3}{A} > \frac{16\rho \sqrt{\epsilon_r} \epsilon_0 c}{\pi}$.

$$\frac{\pi^4 c^2 \epsilon_r \epsilon_0^2 \rho^2 A^2}{128d^3} < t^3 < \left(\frac{\pi^3 c \sqrt{\epsilon_r} \epsilon_0 \rho A}{64d^2} \right)^3 \quad (25)$$

and the relations which f_B falls within the conditions of eqn(22), where the case (i)-(α), (ii)-(α) or (ii)-(β) in Fig. 4, are

$$\begin{cases} \frac{t^3}{A} \leq \frac{16\rho \sqrt{\epsilon_r} \epsilon_0 c}{\pi} \text{ and } t > \frac{32d}{\pi^2} \\ \frac{t^3}{A} > \frac{16\rho \sqrt{\epsilon_r} \epsilon_0 c}{\pi} \text{ and } t \leq \frac{\pi^3 c \sqrt{\epsilon_r} \epsilon_0 \rho A}{64d^2} \end{cases} \quad (26)$$

using eqn(20), (21), (22) with $f = f_B$ of eqn(19). Note that $\frac{\pi^4 c^2 \epsilon_r \epsilon_0^2 \rho^2 A^2}{128d^3} < \left(\frac{\pi^3 c \sqrt{\epsilon_r} \epsilon_0 \rho A}{64d^2} \right)^3$ is always true when $\frac{t^3}{A} > \frac{16\rho \sqrt{\epsilon_r} \epsilon_0 c}{\pi}$. Here, the conditions of eqn(25) is included in the conditions of both eqn(24) and (26). Thus, $|Z_{shf}/Z_{cap}| = 1$ occurs at three frequencies if eqn(25) holds, as shown in Fig. 4(ii)-(β). In this case, the boundary frequency above which the stub input impedance is lower than the capacitor input impedance is the frequency of f_{Bc} in Fig. 4(ii)-(β). Therefore, the boundary frequency for the condition of eqn(25) is merged into the condition of eqn(26), in other words the case (ii)-(β) is merged into the case (ii)-(α), and results to

$$f_B = \frac{\pi c^2 \epsilon_0 \rho}{8td} \quad \text{if} \quad (27)$$

$$\begin{cases} \frac{t^3}{A} \leq \frac{16\rho \sqrt{\epsilon_r} \epsilon_0 c}{\pi} \text{ and } t \leq \frac{32d}{\pi^2} \\ \frac{t^3}{A} > \frac{16\rho \sqrt{\epsilon_r} \epsilon_0 c}{\pi} \text{ and } t > \frac{\pi^3 c \sqrt{\epsilon_r} \epsilon_0 \rho A}{64d^2} \end{cases} \quad (28)$$

$$f_B = \frac{\pi^3 c^2 \epsilon_0 \rho}{256d^2} \quad \text{if} \quad (29)$$

$$\begin{cases} \frac{t^3}{A} \leq \frac{16\rho \sqrt{\epsilon_r} \epsilon_0 c}{\pi} \text{ and } t > \frac{32d}{\pi^2} \\ \frac{t^3}{A} > \frac{16\rho \sqrt{\epsilon_r} \epsilon_0 c}{\pi} \text{ and } t \leq \frac{\pi^3 c \sqrt{\epsilon_r} \epsilon_0 \rho A}{64d^2} \end{cases} \quad (30)$$

The stub input impedance becomes smaller than the decoupling capacitor input impedance above the boundary frequency f_B , and if the LSI operating frequency is higher than the boundary frequency, the stub suppresses the noise more efficiently than the decoupling capacitor with the same required area.

2.3 Numerical Analysis

In order to validate the analysis above, the numerical calculation was carried out as follows. For the given area A , the wire thickness t , the distance d , the resistivity ρ and the relative dielectric constant ϵ_r , the stub length is decided for a given frequency f from eqn(5). The stub width w is decided by eqn(6). Then the inductance L and the capacitance C per unit length of this structure are extracted using Raphael 2D field solver [8]. The resistance R per unit length is extracted using FastHenry [9] 3D field solver in which the resistance and the skin effects are taken into consideration. Then we

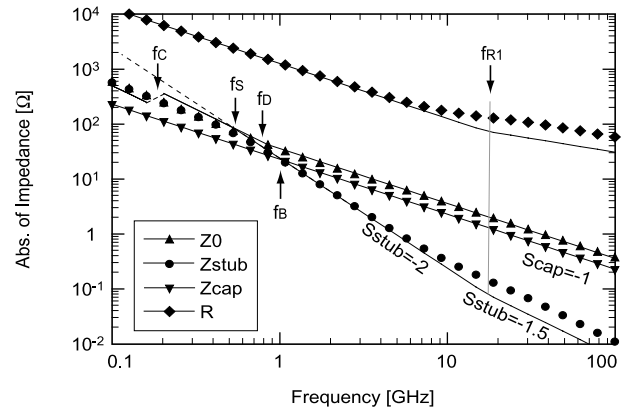


Fig. 5 Frequency dependence of the characteristic impedance, the stub and the capacitor input impedance, and the stub resistance per unit length. The parameter values are $d = 5 \mu\text{m}$, $t = 1 \mu\text{m}$, $A = 1 \text{mm}^2$, $\epsilon_r = 3.9$, $\rho = 1.673 \times 10^{-8} \Omega\cdot\text{m}$.

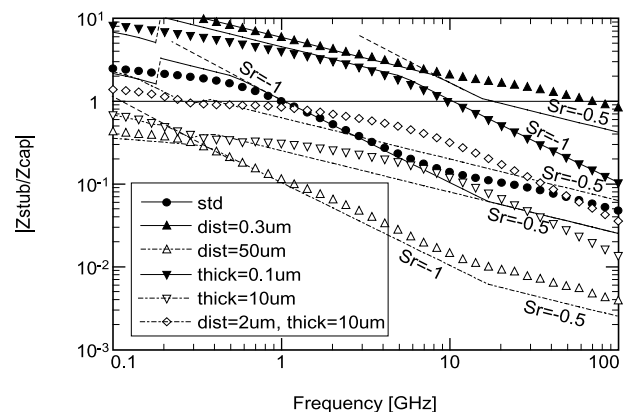


Fig. 6 Input impedance ratio of the stub and the decoupling capacitor with changing a parameter. The standard parameters are $d = 5 \mu\text{m}$, $t = 1 \mu\text{m}$, $A = 1 \text{mm}^2$, $\epsilon_r = 3.9$, $\rho = 1.673 \times 10^{-8} \Omega\cdot\text{m}$.

estimate the stub input impedance by eqn(1)–(4), and the capacitor input impedance is calculated by eqn(15).

The frequency dependence of the characteristic impedance, the stub and the capacitor input impedance, and the resistance per unit length are shown in Fig. 5, where $d = 5 \mu\text{m}$, $t = 1 \mu\text{m}$, $A = 1 \text{mm}^2$, in SiO_2 $\epsilon_r = 3.9$ with Cu wire $\rho = 1.673 \times 10^{-8} \Omega\cdot\text{m}$, are used here as an example. The markers are numerical simulation results and the lines are the analytical results, showing that the analytical models agree well with the numerical simulation results. Note that the step at f_c comes from the discontinuity of the capacitor model expressed by eqn(8). Figure 6 shows the frequency dependence of the stub and the capacitor input impedance ratio with different parameter values. The dashed lines are using $Z_{stub} = Z_{shf}$ even for $f < f_s$, showing that eqn(17) holds. The slope of the stub input impedance is $S_{stub} = -2$ and -1.5 for $f_s \leq f \leq f_R$ and $f_R < f$, the slope of the capacitor impedance is $S_{cap} = -1$, as predicted from eqn(5), (7), (13) and (15). Then S_r , the slope of the $|Z_{stub}/Z_{cap}|$, is -1 and -0.5 for $f \leq f_R$ and $f_R < f$, respectively. These results indicate that the stub structure becomes more efficient over

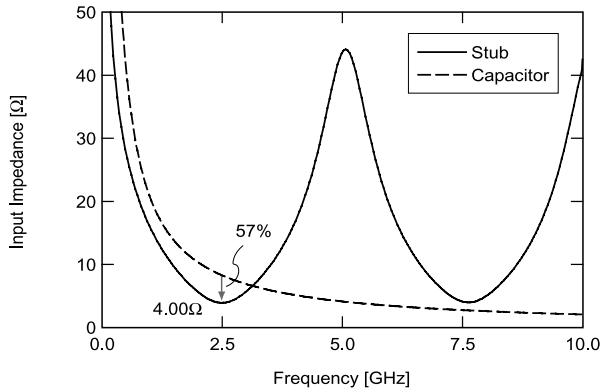


Fig. 7 Frequency dependence of the input impedance of the stubs designed for 2.5 GHz and the capacitor.

the capacitor as the frequency goes higher.

The stub with $d = 5\mu\text{m}$, $t = 1\mu\text{m}$, $A=1\text{mm}^2$, $\epsilon_r=3.9$, $\rho = 1.673 \times 10^{-8}\Omega\cdot\text{m}$ is adjusted for a 2.5 GHz operation LSI as our theoretical test case whose stub structure becomes $w=66\mu\text{m}$, $l=15.181\text{mm}$, $L=83.9\text{nH/m}$, $C=517\text{pF/m}$, $R=532\Omega/\text{m}$ and $C_{total}=6.91\text{pF}$. The frequency dependence of the input impedance of the stub and the capacitor with this structure are shown in Fig. 7. This graph also shows that the stub input impedance is smaller than the capacitor impedance around the designed frequency.

In order to confirm that the stub suppresses the power supply noise better than the decoupling capacitor when $|Z_{stub}/Z_{cap}| < 1$, circuit simulation results using this stub will be given in the next section.

3. Circuit Simulation

3.1 Internal Circuit

A PRBS (Pseudo Random Bit Stream) $2^7 - 1$ generation circuit with an inverter chain at each output of the DFF, as shown in Fig. 8, is used as our test internal circuit. The circuit represents a common synchronous circuit. The PRBS pattern and the inverter chains represent the random switching of the LSI and the combination logics, respectively. The length of the inverter chains distributes from 2 to 12, which represents a path length distribution between DFFs.

We tested three types of power line structures as the reference: nothing attached, the decoupling capacitor and the stub. The inductance of the lead frame and the bonding wire is assumed to be 1 nH, as shown in Fig. 8.

3.2 Simulation Results

Figure 9(a) shows the HSPICE simulation waveforms of the *virtualVdd* node in Fig. 8 for each of the three power line structures, and (b) shows the corresponding spectrum, at 1.8 V 2.5 GHz operation. The standard deviation σ from the *idealVdd* value is used as a measure of the noise amplitude.

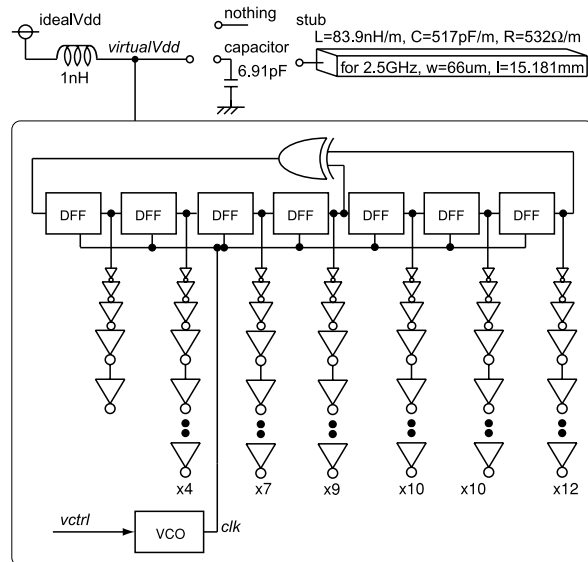


Fig. 8 Internal circuit. A PRBS generator and inverter chains with three kinds of power line structures.

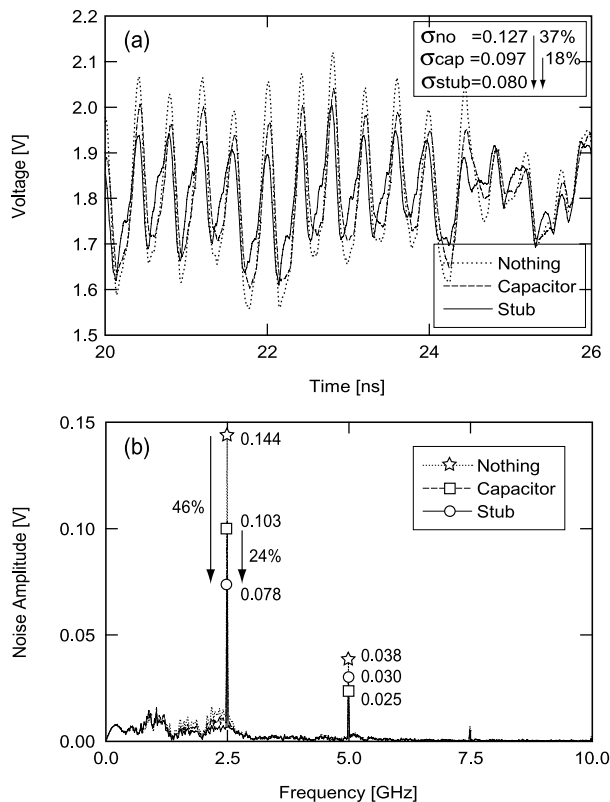


Fig. 9 (a) Simulated waveforms of the *virtualVdd* node. (b) Corresponding spectrum.

$$\sigma = \sqrt{\frac{1}{T} \int_{t_0}^{T+t_0} (V_{virtualvdd} - V_{idealvdd})^2 dt} \quad (31)$$

where T is $2^7 - 1 = 127$ clock cycle period. The σ values are 0.127, 0.097, 0.080 for the nothing, capacitor, stub case respectively. This means that the stub suppressed 37%,

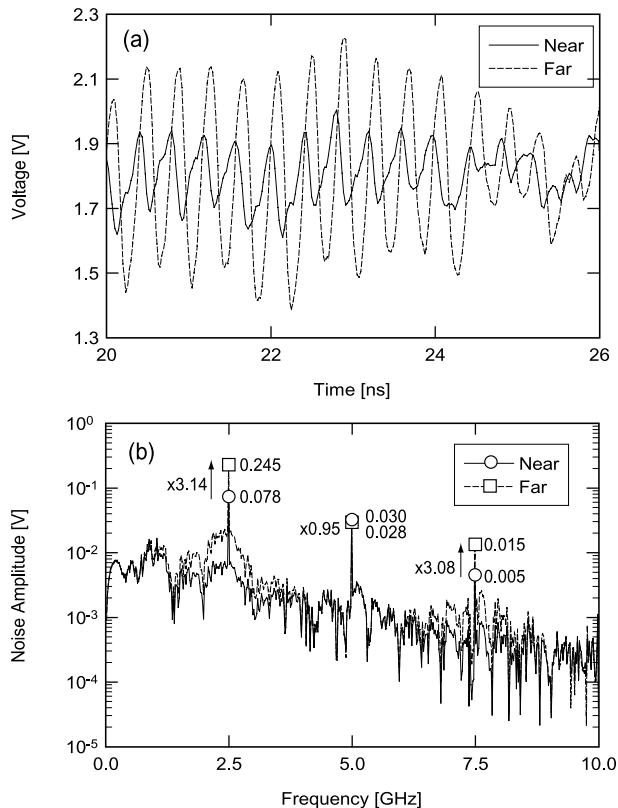


Fig. 10 (a) Waveforms of the near end (virtualVdd) and the far end of the stub. (b) The corresponding spectrum of the far end voltage.

18% of the noise compared with the nothing, capacitor case. Also, the stub suppressed 46%, 24% of the 2.5 GHz noise component compared with the nothing, capacitor case, respectively, as shown in Fig. 9(b).

The above power supply noise reduction ratios are not equal to the input impedance ratio (57%) of the stub and the decoupling capacitor since the power supply noise depends not only on the stub or the capacitor input impedance but also the parasitic impedance of the package and the parasitic capacitor of the internal circuit, and so on.

3.3 Voltage Swing at the End Terminal

The stub suppresses the noise because it stores and provides the energy of the designed frequency so that the less AC current component goes through the lead frame and the bonding wire inductance. The energy is stored by swinging the signal voltage in the stub, and the far end terminal has the maximum voltage amplitude. The ratio of the AC voltage amplitudes at the near end and the far end is

$$\frac{V_{far}}{V_{near}} \approx -j \frac{1 + \eta}{1 - \eta} \quad (32)$$

at the steady state, where η is the round trip attenuation factor $e^{-\alpha \cdot 2l}$. The ratio is 3.38 on our stub. When the stub is used in an LSI, the attention should be paid so as not to exceed the break down voltage of the insulator between

the metal layers, since the voltage at the end terminal becomes higher than the supply voltage. Since the stub input impedance is insensitive with the distance d between the signal and the gnd, the thickness of the insulator could be increased if needed.

Figure 10(a) shows the simulated waveforms of the near end and the far end of the stub, and (b) shows the corresponding spectrum. These graphs show that the stub far end voltage has 3.14 and 3.08 times larger voltage swing than the near end around 2.5 GHz and 7.5 GHz, respectively, which means that the stub stores the energy around the frequencies, not around 5 GHz. The result agrees with the frequency dependence of the stub shown in Fig. 7, and the theoretical value from eqn(32) of 3.38.

4. Discussion

4.1 Time Constant

The input impedance of the stub is Z_0 at the initial state, and Z_{stub} at the steady state. It needs time constant τ to change the input impedance from Z_0 to Z_{stub} . Since the the near end impedance Z_s is connected in parallel to the stub for the noise source current I_0 , the current of the forward-going wave I_f in the stub at the initial condition is,

$$I_f(t = 0) = \frac{Z_s}{Z_s + Z_0} I_0. \quad (33)$$

Since the forward-going wave is increased at the reflections which occur every half clock period $1/2f$, the current I_f at a time t becomes

$$I_f = \frac{Z_s}{Z_s + Z_0} \{1 + (-\eta\Gamma_s) + \dots + (-\eta\Gamma_s)^{2ft}\} I_0 \quad (34)$$

$$= \frac{Z_s}{Z_s + Z_0} \cdot \frac{1 + \eta\Gamma_s(-\eta\Gamma_s)^{2ft}}{1 + \eta\Gamma_s}. \quad (35)$$

where $\Gamma_s = (Z_s - Z_0)/(Z_s + Z_0)$ is the reflection coefficient at the near end, η is the round trip attenuation factor $e^{-\alpha \cdot 2l}$, the round trip phase rotation is π and $e^{-j\pi} = -1$. Here,

$$(-\eta\Gamma_s)^{2ft} = e^{2ft \log |-\eta\Gamma_s|} e^{j2ft\theta} \quad (36)$$

using $a^{bx} = e^{bx \log a}$ and $\log z = \log |z| + j \arg z$. It shows that the time constant is expressed as

$$\tau = \frac{1}{-2f \log |\eta\Gamma_s|}. \quad (37)$$

The current of the backward-going wave has the same time constant, so that the voltage and impedance of the stub have the same time constant as well. Note that $|\eta\Gamma_s| \leq 1$, $\log |\eta\Gamma_s| \leq 0$ and τ is positive. The time constant is 453 ps which is less than two clock cycle in our test case.

4.2 Frequency Components

If all the gates would switch at the same timing in every clock cycle, the current would contain only nf_0 components.

However, practical circuits switch randomly at each clock cycle and cause non- nf_0 components. These components are suppressed more robustly by the capacitor. In addition, the capacitor may suppress the higher order nf_0 components better than the stub, as shown in Fig. 7 other than around 2.5 GHz, and even 7.5 GHz case.

The stub reduces the power supply noise better than the capacitor since f_0 component is dominant in this example. However, if the non- nf_0 components or the higher order frequencies increase, the decoupling capacitor is better than the stub.

4.3 Higher Frequency Case

Since the stub length $l \propto f^{-1}$, the stub width $w \propto f$, and the skin depth $\delta < f^{-0.5}$, the stub input impedance becomes $Z_{stub} = Rl/2 \propto f^{-2}$ or $f^{-1.5}$ before and after f_R at which skin effect starts to appear, while the capacitor input impedance becomes $Z_{cap} \propto f^{-1}$. The ratio becomes $|Z_{stub}/Z_{cap}| \propto f^{-1}$ or $f^{-0.5}$, as shown in in Sect. 2. Therefore the stub has more advantage over the capacitor as the operating frequency goes higher, as shown in Figs. 5 and 6.

The stub input impedance Z_{stub} in our example is 4.00Ω while $|Z_{cap}| = 9.22$ and $|Z_{stub}/Z_{cap}| = 0.43$ at 2.5 GHz with $A=1 \text{ mm}^2$. If the frequency becomes 10 times higher, 25 GHz for example, with the same d , t , A , ϵ_r and ρ , the impedances become $Z_{stub} = 0.089$, $|Z_{cap}| = 0.922$, $|Z_{stub}/Z_{cap}| = 0.097$ and show that the stub advantage ratio increases $0.43/0.097=4.43$ times which is in between $10^{0.5} \sim 10^1$. When the distance d is reduced to $1 \mu\text{m}$, the impedances become $Z_{stub} = 0.091$, $Z_{cap} = 0.184$ and the stub still keeps the advantage over the capacitor at this frequency.

The capacitance per unit area may be increased by using lateral capacitors together with the vertical capacitors, such as a comb capacitor [10], depending on d , t and the line-to-line space. However, the frequency dependence of the capacitor input impedance $Z_{cap} \propto f^{-1}$ is the same and the advantage of the stub at high frequency still holds.

4.4 Stub Usage

The stub is designed on-chip in this paper. On-package or on-PCB board stubs can also suppress the noise. A smaller resistance stub using a thicker metal layer of the package or of the PCB board can realize more effective noise suppression. However, the parasitic inductance of the lead frame and the bonding wire could be the noise source when the on-package or on-PCB board stubs are used.

Some devices, especially mobile ones, require dynamic operating frequency control, and the stub length should be adjusted in accordance with the operating frequency in such cases. A variable inductor or capacitor on the stub end termination instead of the open termination can virtually control the stub length by changing the phase rotation at the reflection.

5. Conclusion

The stub and the capacitor have been compared for power supply noise reduction. A quarter-length stub attached to the power supply line of an LSI chip works as a band-eliminate filter, and suppresses the power supply bounce of the designed frequency. The boundary frequency above which the stub is more effective than the same-area decoupling capacitor is clarified.

The circuit simulation results show that the stub reduces 37% and 18% of the power supply noise compared with the nothing attached case, and decoupling capacitor case, respectively, in our 1.8 V 2.5 GHz test circuit with $d = 5 \mu\text{m}$, $t = 1 \mu\text{m}$, $A=1 \text{ mm}^2$, $\epsilon_r=3.9$, $\rho = 1.673 \times 10^{-8} \Omega \cdot \text{m}$ case.

Theoretical study shows that the stub will have more advantage over the capacitor, and the stub on-chip integration will be possible in higher frequency operation LSIs.

Acknowledgement

This study was supported by Grant-in-Aid for JSPS Fellows of the Ministry of Education, Culture, Sports, Science and Technology.

References

- [1] M. Badaroglu, K. Tiri, S. Donnay, P. Wambacq, I. Verbauwhede, G. Gielen, and H.D. Man, "Clock tree optimization in synchronous CMOS digital circuits for substrate noise reduction using folding of supply current transients," Proc. ACM/IEEE Design Automation Conf., pp.399–404, June 2002.
- [2] H. Tohya, "New technologies doing much for solving the EMC problem in the high performance digital PCBs and equipment," IEICE Trans. Fundamentals, vol.E82-A, no.3, pp.450–456, March 1999.
- [3] T. Nakura, M. Ikeda, and K. Asada, "Theoretical study of stubs for power line noise reduction," Proc. IEEE Custom Integrated Circuits Conf., pp.715–718, Sept. 2003.
- [4] T. Nakura, M. Ikeda, and K. Asada, "Preliminary experiments for power supply noise reduction using stubs," Proc. IEEE Asia-Pacific Conf. on Advanced System Integrated Circuits, pp.286–289, Aug. 2004.
- [5] P. Heydari, S. Abbaspour, and M. Pedram, "A comprehensive study of energy dissipation in lossy transmission lines driven by CMOS inverters," Proc. IEEE Custom Integrated Circuits Conf., pp.517–520, May 2002.
- [6] D.K. Cheng, Fundamentals of Engineering Electromagnetics, Addison-Wesley Series in Electrical Engineering, Chap.3-11, 1994.
- [7] A.R. Djordjevic, A.G. Zajic, D.V. Tosic, and T. Hoang, "A note on the modeling of transmission-line losses," IEEE Trans. Microw. Theory Tech., vol.51, no.2, pp.483–486, Feb. 2003.
- [8] "Raphael USER'S GUIDE," [Online] <http://www.synopsys.com>
- [9] "FastHenry USER'S GUIDE," [Online] Available: <http://rleweb.mit.edu/vlsi/codes.htm>
- [10] A. Imamura, M. Fujishima, and K. Hoh, "Bending-comb capacitor with a small parasitic inductance," IEEE/JSAP Symposium on VLSI Circuits, pp.22–25, June 2002.



Toru Nakura was born in Fukuoka, Japan in 1972. He received the B.S., and M.S. degree in electronic engineering from the University of Tokyo, Tokyo, Japan, in 1995 and 1997 respectively. Then he worked as a high-speed communication circuit designer using SOI devices for two years, and worked as a EDA tool developer for three years. He joined the University of Tokyo again as a Ph.D. student in 2002. His current interest includes signal integrity on high-speed operation LSI circuits.



Makoto Ikeda received the B.S., M.S., and Ph.D. in electronics engineering from the University of Tokyo, Tokyo, Japan, in 1991, 1993, and 1996, respectively. He joined the Department of Electronic Engineering, the University of Tokyo as a Faculty Member in 1996, and is currently an Associate Professor at VLSI Design and Education Center, the University of Tokyo. His research interests include the reliability of VLSI design. He is a member of the Institute of Electrical and Electronics Engineers (IEEE),

CEJ, and the Information Processing Society of Japan (IPSJ).



Kunihiro Asada was born in Fukui, Japan, on June 16, 1952. He received the B.S., M.S., and Ph.D. in electronic engineering from the University of Tokyo in 1975, 1977, and 1980, respectively. In 1980 he joined the Faculty of Engineering, the University of Tokyo, and became a lecturer, an associate professor and a professor in 1981, 1985 and 1995, respectively. From 1985 to 1986 he stayed in Edinburgh the University as a visiting scholar supported by the British Council. From 1990 to 1992 he served as

the first Editor of English version of IEICE (Institute of Electronics, Information and Communication Engineers of Japan) Transactions on Electronics. In 1996, he established VDEC (VLSI Design and Education Center) with his colleagues in the University of Tokyo. It is a center supported by the Government to promote education and research of VLSI design in all the universities and colleges in Japan. He is currently in charge of the head of VDEC. His research interests are design and evaluation of integrated systems and component devices. He has published more than 400 technical papers in journals and conference proceedings. He has received Best Paper Awards from IEEJ (Institute of Electrical Engineers of Japan), IEICE and ICMTS1998/IEEE and so on. He is a member of the Institute of Electrical and Electronics Engineers (IEEE), and the Institute of Electrical Engineers of Japan (IEEJ).